# SUPPLEMENTAL MATERIAL
## A model of representational spaces in human cortex
Guntupalli, Hanke, Halchenko, Connolly, Ramadge, Haxby

*S.1. Methods: Details about MRI scanning protocols and data preprocessing*

*S.1.1. Movie study*

*S.1.1.1. fMRI protocol*. Subjects were scanned in a Philips Intera Achieva 3T scanner with an 8 channel head coil at the Dartmouth Brain Imaging Center. Functional scans were acquired with an echo planar imaging sequence (TR=2.5 s, TE=35 ms, flip angle=90°, 80 x 80 matrix, FOV=240 mm x 240 mm) every 2.5 s with whole brain coverage (41x3 mm thick interleaved axial slices). We acquired a total of 2718 functional scans with 1350 TRs in four runs during the first session and 1368 TRs in four runs during the second session. T1-weighted anatomical scans were acquired at the end of each session (MPRAGE, TR=9.85 s, TE=4.53 s, flip angle=8°, 256 x 256 matrix, FOV=240 mm, 160 1 mm thick sagittal slices). The voxel resolution was 0.938 mm x 0.938 mm x 1.0 mm.

*S.1.1.2. fMRI data preprocessing*. Each subject's fMRI data were preprocessed using AFNI software (Cox, 1996; http://afni.nimh.nih.gov). Functional data were corrected for the order of slice acquisition then for head motion by aligning to the last volume of the last functional run. Any spikes in the data were removed using 3dDespike in AFNI. Data were then filtered using 3dBandpass in AFNI to remove any temporal signal variation slower than 0.00667 Hz, faster than 0.1 Hz, and that correlated with the whole brain average signal or the head movement parameters. Residual data were then aligned to the MNI 152 brain template using nearest neighbor resampling and spatially smoothed with a 4 mm full-width-at-half-maximum (FWHM) Gaussian filter. These were the anatomically-aligned data used for comparison during validation analyses. Data acquired during the overlapping movie segments were discarded resulting in a total of 2662 TRs with 1326 TRs in the first session and 1336 TRs in the second session. We derived a gray matter mask by segmenting the MNI_avg152T1 brain provided in AFNI and removing any voxel that was outside the cortical surface by more than twice the thickness of the gray matter at each surface node. It included 54,034 3 mm isotropic voxels across both hemispheres. We used this mask for all subsequent analyses of all subjects. We implemented our methods and ran our analyses in PyMVPA unless otherwise specified (Hanke et al. 2009; http://www.pymvpa.org). All preprocessing and analyses were carried out on a 64-bit Debian 7.0 (wheezy) system with additional software from NeuroDebian (Halchenko and Hanke, 2012; http://neuro.debian.net).

*S.1.2. Animal species perception study*

*S.1.2.1. fMRI protocol*. Subjects were scanned in a Philips Intera Achieva 3T scanner with an 8 channel head coil at the Dartmouth Brain Imaging Center. T1-weighted anatomical scans were acquired at the end of each session (MPRAGE, TR=9.85 s, TE=4.53 s, flip angle=8°, 256 x 256 matrix, FOV=240 mm, 160 1 mm thick sagittal slices). The voxel resolution was 0.938 mm x 0.938 mm x 1.0 mm. Functional scans were acquired with an echo planar imaging sequence (TR=2 s, TE=35 ms, flip angle=90°, 80 x 80 matrix, FOV=240 mm x 240 mm) every 2 s with whole brain coverage (42x3 mm thick interleaved axial slices).

*fMRI data preprocessing*. Each subject's fMRI data were preprocessed using AFNI software (Cox, 1996; http://afni.nimh.nih.gov). Functional data were first corrected for the order of slice acquisition and then for head motion by aligning to the last volume of the last functional run. Any spikes in the data were removed using 3dDespike in AFNI. Data were then filtered to remove any linear and quadratic trends. Residual data were then spatially smoothed with a 4 mm full-width at half-max Gaussian filter. We estimated the beta values for each condition in each run by deconvolving with hemodynamic response function using 3dDeconvolve in AFNI. Each run yielded 6 beta values per voxel corresponding to 6 animal species. We then aligned these beta maps first to the mean functional image of the corresponding subject's data from the Raiders study and then to the MNI 152 brain template using the alignment parameters derived in the raiders study using nearest neighbor resampling. These were the anatomically-aligned data used for comparison during validation analyses.

*S.1.3. Retinotopic mapping*

*S.1.3.1. Stimuli*. Subjects viewed high-contrast black and white checkerboard patterns flickering at 8 Hz within symmetrical wedges for polar angle mapping runs and within a ring for eccentricity mapping runs. Each wedge subtended 22.5° at fixation and each ring subtended ~1° of visual angle in width. During polar angle runs, the symmetrical wedge was presented at a given location for 2 s before moving to an adjacent non-overlapping location for the next TR. In clockwise runs, the wedge moved to an adjacent clockwise location and in counter-clockwise runs, it moved to an adjacent counter-clockwise location. During eccentricity runs, each ring was presented for 2 s at a given location centered at the fixation before being replaced by a ring at an adjacent non-overlapping location either outward or inward from the fixation. In expanding runs, the ring moved outward with the outermost ring followed by the innermost ring at the end of the cycle and in the contracting runs, it moved inwards from the outermost location. Each run started with 16 s of fixation followed by wedge or ring stimuli presented for one cycle (360° rotation of wedges, innermost to outermost location of rings) followed by another 16 s of fixation.

*S.1.3.2. fMRI protocol*. Subjects were scanned in a Philips Intera Achieva 3T scanner at the Dartmouth Brain Imaging Center. Functional scans were acquired with an echo planar imaging sequence (TR=2 s, TE=35 ms, flip angle=90°, 128 x 128 matrix, FOV=240 mm x 240 mm) with 1.875 mm x 1.875 mm in-plane resolution covering early visual cortex in a slab aligned parallel to the calcarine sulcus (30 x 2 mm thick interleaved axial slices). T1-weighted anatomical scans were acquired at the end of each session (MPRAGE, TR=9.85 s, TE=4.53 s, flip angle=8°, 256 x 256 matrix, FOV=240 mm, 160 1 mm thick sagittal slices). The voxel resolution was 0.938 mm x 0.938 mm x 1.0 mm. Five subjects were scanned with an 8 channel head coil and three subjects were scanned with a 32 channel head coil with the identical protocol.

*S.1.3.2. fMRI preprocessing.* Each subject's fMRI data was preprocessed using AFNI software (Cox, 1996; http://afni.nimh.nih.gov). Functional data were first corrected for the order of slice acquisition. Each volume was aligned to the last volume of the last functional run to correct for head motion. Any spikes in the data were removed using 3dDespike in AFNI. Data were then filtered to remove any linear and quadratic trends. Residual data was then spatially smoothed with a 4 mm full-width at half-max Gaussian filter. We averaged the voxel time series data from

the repeated runs of the same kind to generate one dataset for each condition (clockwise and counter-clockwise wedges, expanding and contracting rings).

*S.1.3.3. Estimation of retinotopic maps*. We estimated the polar angle and eccentricity maps from the average datasets using 3dRetinoPhase in AFNI with DELAY method for phase estimation. Retinotopic maps for each subject were aligned to the functional brain template from the movie for that subject and resampled to 3 mm isotropic voxels in the process, and then to the MNI 152 brain template using the alignment parameters derived in the Raiders study using nearest neighbor resampling. We then generated spatial tuning maps of polar angle and eccentricity field maps for each subject. The polar angle tuning map has an 18 dimensional vector at each voxel, corresponding to polar angles from 0° to 170° in steps of 10° (0° is the vertical meridian and 90° is the horizontal meridian), with the values for dimensions defining a cosine curve with 1 for that voxel's preferred polar angle and -1 for the orthogonal polar angle. We computed the values for each dimension as cosine(2*(PPA-VPA)) for each voxel, where PPA is the preferred polar angle for that voxel as determined by retinotopic mapping and VPA is the polar angle for that vector dimension. For example, if a voxel's measured preferred polar angle is 40°, the value for the dimension corresponding to 40° is 1 and for 130° is -1. We applied a similar procedure to generate eccentricity tuning maps using the transformation: 1-abs(exp(PEA/360)-exp(VEA/360)), where PEA is the that voxel's preferred eccentricity and VEA is the eccentricity for the vector dimension.

*S.1.4. Category-selective localizer*

*S.1.4.1. Stimuli and design.* Subjects viewed still images from 6 categories – human faces, human bodies without heads, small objects, houses, outdoor scenes, and scrambled images – in a block design. During each block, we presented 16 images from a category with 900 ms of image presentation and 100 ms of ISI. Subjects performed a one-back repetition detection task by reporting when an image repeated in succession. There were 8 s of inter-block interval during which subjects performed a fixation color change detection task. Each run started with 12 s of fixation in the beginning and consisted of 12 blocks with each category represented twice and 12 s of fixation at the end. Each subject participated in a total of 4 runs.

*S.1.4.2. fMRI protocol*. Subjects were scanned in a Philips Intera Achieva 3T scanner at the Dartmouth Brain Imaging Center. Functional scans were acquired with an echo planar imaging sequence (TR=2 s, TE=35 ms, flip angle=90°, 80 x 80 matrix, FOV=240 mm x 240 mm) every 2 s with whole brain coverage (42x3 mm thick interleaved axial slices). T1-weighted anatomical scans were acquired at the end of each session (MPRAGE, TR=9.85 s, TE=4.53 s, flip angle=8°, 256 x 256 matrix, FOV=240 mm, 160 1 mm thick sagittal slices). The voxel resolution was 0.938 mm x 0.938 mm x 1.0 mm. All the subjects except one were scanned using an 8 channel head coil and one subject with a 32 channel head coil with an identical protocol.

*S.1.4.3. fMRI data preprocessing.* Each subject's fMRI data was preprocessed using AFNI software (Cox, 1996; http://afni.nimh.nih.gov). Functional data was first corrected for the order of slice acquisition and head motion by aligning to the last volume of the last functional run. Any spikes in the data were removed using 3dDespike in AFNI. Data was then filtered to remove any linear and quadratic trends.

*S.1.4.4. Mapping category-selective topographies.* We used general linear model (GLM)

analysis to define category-selective topographies for the following contrasts: faces (human faces - objects and scrambled images; Kanwisher, 2010; Grill-Spector and Weiner, 2014; Haxby et al. 1999, 2000), places (houses and scenes - faces and scrambled images; Epstein and Kanwisher, 1998), objects (small objects - scrambled images Malach et al. 1995), and bodies (human bodies - objects and scrambled images; Downing et al. 2001; Peelen and Downing, 2005). The preprocessed data from the category-selectivity experiment of each subject was smoothed with a 6 mm full-width at half-max Gaussian filter. These data also were rotated into the common model space, as derived from all of the movie data. Individual data for every subject was then rotated into the anatomical voxel space of every other subject. Thus, anatomical space of each subject was occupied by that subject's data and by the data from all other subjects. The group data in each anatomical space was resampled into a curvature-aligned standard cortical surface mesh (ico64 with 81,942 nodes). For each subject, category-selective t-statistic maps were computed for each contrast using 3dDeconvolve and 3dREMLfit in AFNI on on that subject's data in his or her curvature-aligned cortical space, for the average of all other subjects' data (N-1) that was projected into that subject's cortical space via the common model, and for the average of all other subjects' data (N-1) in curvature-based anatomically-aligned cortical space. We calculated correlations between the t-statistic maps calculated from subjects' own data and those calculated from other subjects' data in anatomically-aligned cortex and hyperaligned cortex.

*S.2. Results: More on hyperalignment*

*S.1.1. Between-subject correlations of neural responses*

We asked if hyperalignment increased between-subject correspondence of univariate measures of local neural responses. We computed correlations of time-series between each subject and the mean of other subjects in each voxel or feature before and after hyperalignment in each movie half. Features of hyperaligned model dimensions are illustrated by mapping between-subject correlations of model dimensions into the anatomy of one subject. Hyperalignment increased the between-subject correlation of single feature tuning profiles in occipital, temporal, parietal, and lateral prefrontal cortices. Hyperalignment increased mean correlation across subjects across all cortical features from 0.169 to 0.322 (95% CI of bootstrapped difference: [0.135, 0.165]). As in all validation tests on movie data, the common model space and transformation matrices were derived from one half of the movie data and then applied to the other half for cross-validated tests, in this case between-subject correlations of time series.

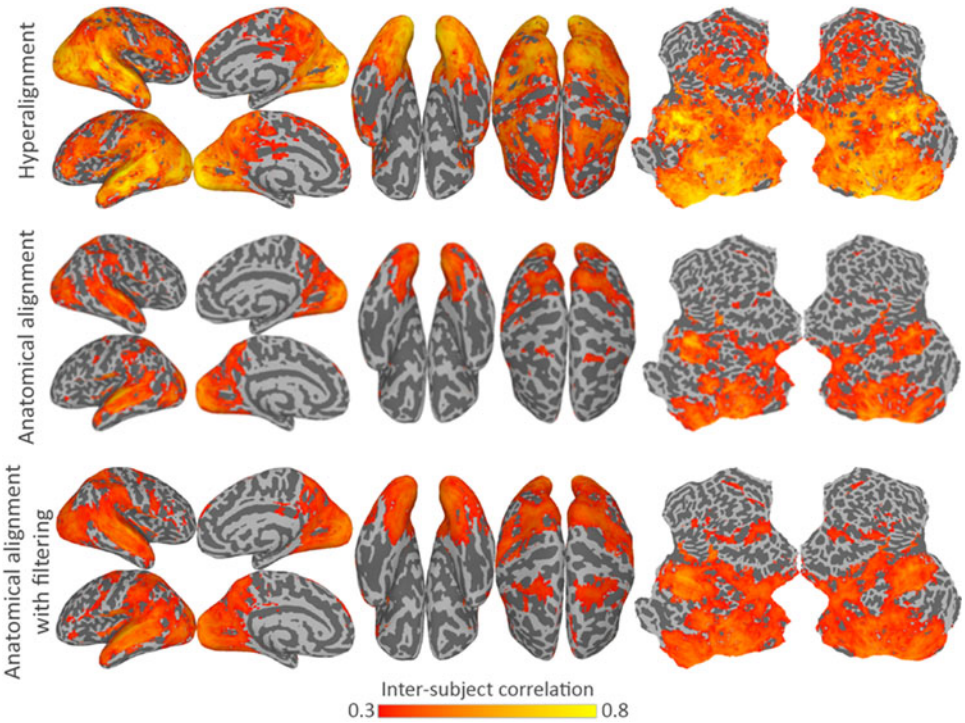


Supplementary Figure S1. Between-subject correlation of neural response profiles. Univariate voxel-by-voxel correlation of response profiles across subjects while they watched the movie after whole cortex hyperalignment (top), as compared to after anatomical alignment (middle) and anatomical alignment with control for the effect of filtering (bottom).

In addition, we controlled for the effect of resampling data into a new space using high-dimensional rotations. Hyperalignment resamples data into common model dimensions using high-dimensional rotations, which involves calculating the time-series for each model dimension as a weighted sum of voxels. To achieve a similar level of resampling in anatomically-aligned data, we hyperaligned each subject's data into a common model space derived with different reference subjects, unlike the case of hyperalignment in which all subjects are hyperaligned to a common model space with the same reference subject. The inter-subject correlations of time-series after this control for the effect of filtering are increased, relative to those for standard anatomical alignment, but still far lower than inter-subject correlations of time-series for common model dimensions (Supplementary Figure S1).

*S.1.2. Topographic basis functions for model dimensions*

For illustration, we projected three arbitrary dimensions in the common model derived from the full movie data onto cortical surfaces of two subjects. Transformation matrix vectors for dimensions (matrix columns) are projected back into the cortical anatomical space of two subjects to show their topographies. The searchlight hyperalignment algorithm constrains the topography for a given dimension to voxels in searchlights that contain the location of that dimension in the reference brain. Patterns of response are modeled as weighted sums of overlapping topographic basis functions. Topographic basis functions for each dimension are

distinctive for each individual and associated with response profiles that are common across subjects.

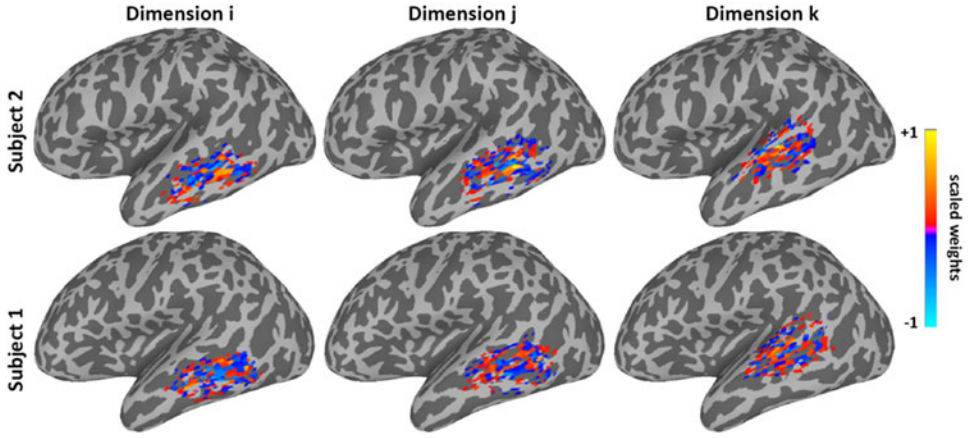


Supplementary Figure S2. Topographic basis functions for three overlapping common model dimensions in the superior temporal sulcus of two subjects.

*S.2. More on bsMVPC*

*S.2.1. Regions of interest (ROI) analyses*

To illustrate the general validity of the qualities of the common model of representational spaces in human cortex, in particular its applicability in different information domains and the extent to which it captures fine-grained topographies, we analyzed the properties of the model in a variety of functionally-defined cortical loci. We selected twenty loci using Neurosynth, a database derived from meta-analysis of over 10,000 fMRI studies (neurosynth.org; Yarkoni et al. 2011). We took the coordinates for the peak location associated with selected terms (Table S1) and analyzed the properties of the model representational spaces that surrounded these loci in searchlights with a 3-voxel radius (mean volume = 119 voxels; Figures 2, 3, 4, 5; Supplemental Figure S11).

Supplementary Table S1. Selected cortical loci from Neurosynth. V1 – primary visual cortex, MT – middle temporal visual motion area, FFA – fusiform face area, PPA – parahippocampal place area.

| Search term | Hemi-sphere | MNI coordinates x | y | z |
|---|---|---|---|---|
| V1 | left | -4 | -82 | -4 |
| | right | 10 | -94 | 2 |
| MT | left | -42 | -72 | 2 |
| | right | 44 | -66 | 2 |
| Visual word form area | left | -46 | -60 | -14 |
| FFA | left | -42 | -52 | -20 |
| | right | 40 | -50 | -22 |
| Scenes (PPA) | left | -26 | -46 | -10 |
| | right | 34 | -38 | -12 |
| Primary auditory (A1) | left | -44 | -30 | 10 |
| | right | 52 | -14 | 4 |
| Voice | left | -60 | -14 | 0 |
| | right | 60 | -4 | -12 |
| Music | left | -52 | -14 | 0 |
| | right | 60 | -20 | 4 |
| Calculations | left | -30 | -66 | 38 |
| | right | 34 | -64 | 44 |
| Broca's area | left | -52 | 14 | 12 |
| Working memory | left | -44 | 26 | 24 |
| | right | 44 | 42 | 26 |

*S.2.2. Whole brain bsMVPC of movie time segments*

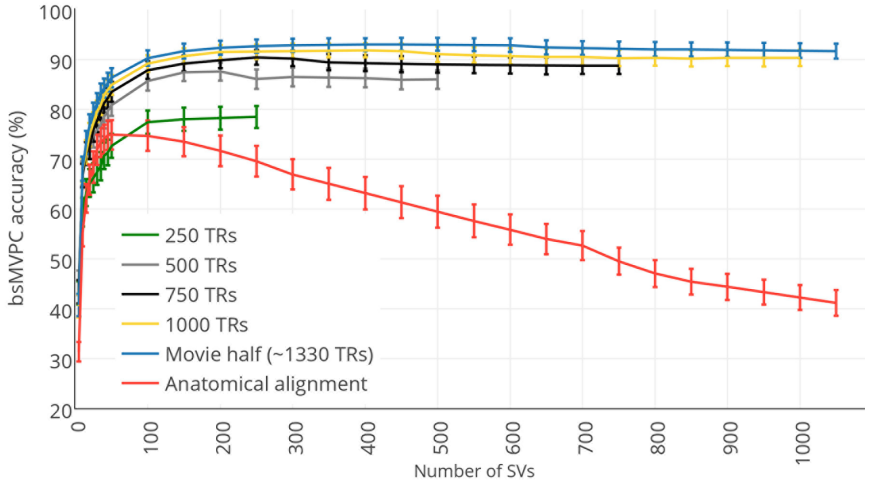


Supplemental Figure S3. Whole cortex bsMVPC of movie time-segments using different numbers of top singular vectors (SVs) from singular vector decomposition and different numbers of time-points to derive hyperalignment transformation matrices. Classification was performed on each movie half separately with hyperalignment transformations derived from the other half. bsMVPC accuracies are shown with hyperalignment transformation matrices calculated from all data in each movie half (~1330 time-points) and from the initial 250, 500, 750, and 1000 time-points in each movie half. Consistent with our previous analysis of ventral temporal cortex (Haxby et al. 2011), 250 time-points (10:25 min) were sufficient to derive hyperalignment parameters to afford bsMVPC accuracies that exceeded bsMVPC of anatomically-aligned data with higher dimensionality and bsMVPC accuracies increase further with each increment in the size of the movie data set. These results suggest that approximately 30 min of movie data are sufficient for deriving a common model that affords whole brain bsMVPC accuracies that greatly exceed bsMVPC of anatomically aligned data (90.4% vs 74.8%) and approach, but do not match, accuracies achieved with a common model based on 55 min of movie data (93.0%).

*S.2.3. bsMVPC of shorter movie time segments.*

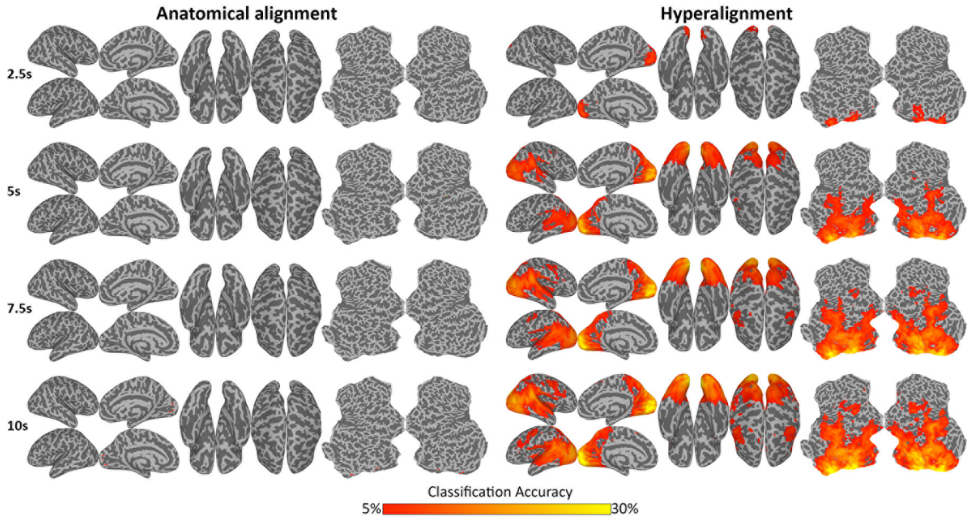


Supplementary Figure S4. Searchlight bsMVPC accuracies for 2.5 s (1 time-point), 5 s (2 time-points), 7.5 s (3 time-points), and 10 s (4 time-points) movie segments after anatomical alignment and after hyperalignment.

*S.2.4. Effect of filtering on bsMVPC of movie time segments.*

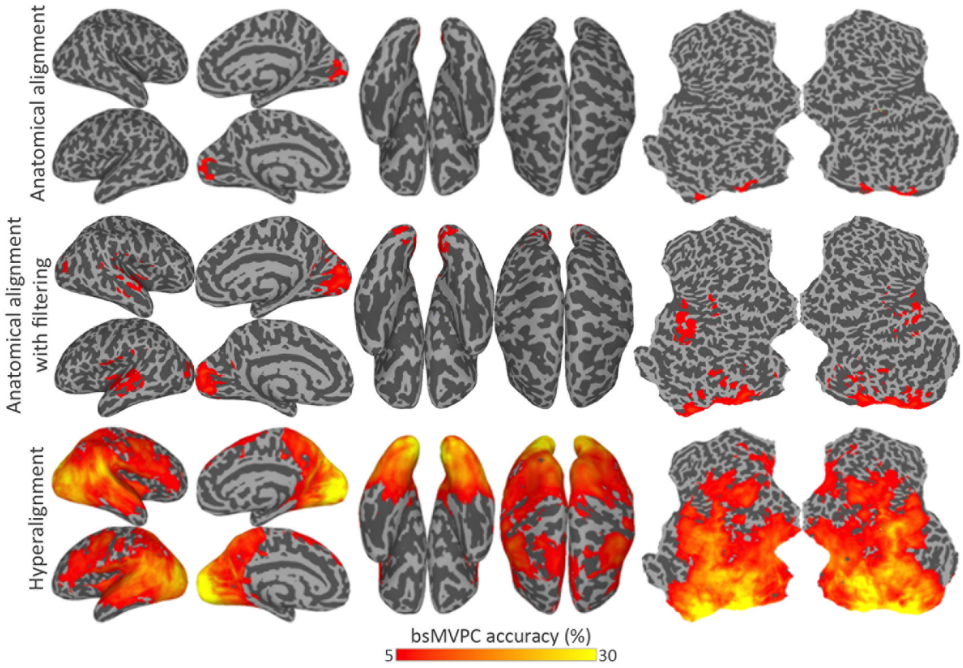


Supplementary Figure S5. Effect of filtering on bsMVPC of anatomically aligned data. Anatomically-aligned data were resampled using high-dimensional rotation as in Supplementary Figure S1 to control for the effect of filtering on bsMVPC accuracies. Note that filtering anatomically-aligned data results in a small improvement in accuracies for bsMVPC of movie time segments that are, nonetheless, far lower than for bsMVPC of data in common model space. The top and bottom panels, showing accuracies of bsMVPC of anatomically-aligned and hyperaligned data, are the same as in Figure 2a and are shown for comparison with bsMVPC of anatomically-aligned data that has been resampled with high-dimensional rotations into the anatomical spaces of other subjects (middle panel).

*S.3. More on representational geometry*

*S.3.1. Effect of hyperalignment on representational geometry*

*S.3.1.1. Stability of within-subject representational similarities.* Our results showed that the between-subject correlation of neural representational geometries during movie viewing increased after hyperalignment. In order to test whether this increase is at the cost of losing individual-specific similarity structures, we computed the correlations of similarity structures within each subject during the test half of the movie in each 3-voxel radius searchlight before and after hyperalignment. Supplemental Figure S6a shows the average of this correlation across both movie halves and across subjects at each cortical location. Across the whole cortex, representational geometry before and after hyperalignment is highly correlated ($r>0.4$), which is higher than the correlation between-subjects. It is clear from these results that the representational similarities are well preserved after hyperalignment at the individual subject level.

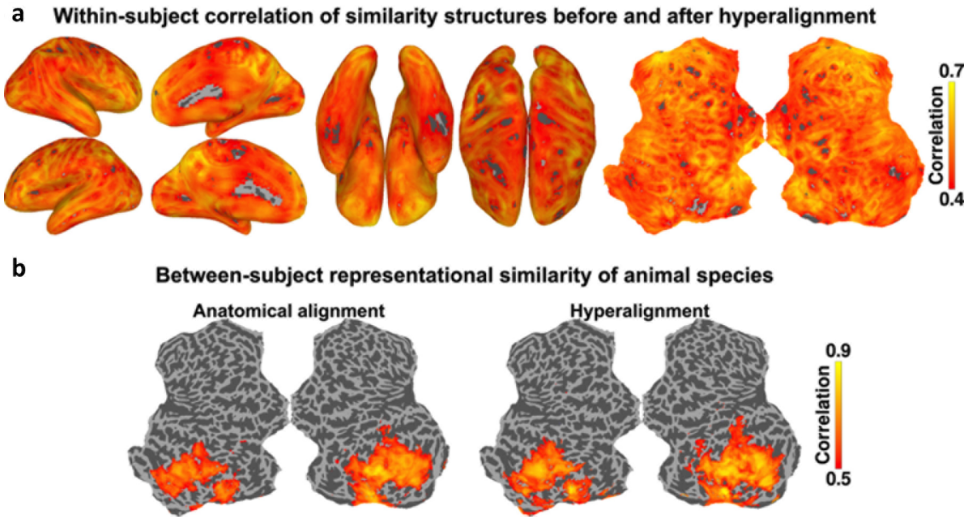


Supplementary Figure S6. Effect of hyperalignment on representational similarity. (a) Within-subject similarity of similarity structures before and after hyperalignment. (b) Between-subject representational similarity of animal species before and after hyperalignment.

*S.3.1.2. Between-subject representational similarities of animal species.* Between-subject representational similarity analysis was performed on data from the animal species perception study using searchlights of 3 voxel radius. In each searchlight, each subject's neural similarity structure was correlated with the average of other subjects' neural similarity structures in that searchlight. This was performed on data aligned based on anatomy and the data in common model derived from the movie data. Supplemental Figure S6b shows the results mapped onto flattened cortex. ISCs are higher after movie-based hyperalignment than after anatomical alignment, indicating better alignment of searchlight-by-searchlight variation in representational geometry for this restricted stimulus domain.

*S.4. More on spatial resolution of model space*

*S.4.1. Full brain maps of the effect of smoothing*

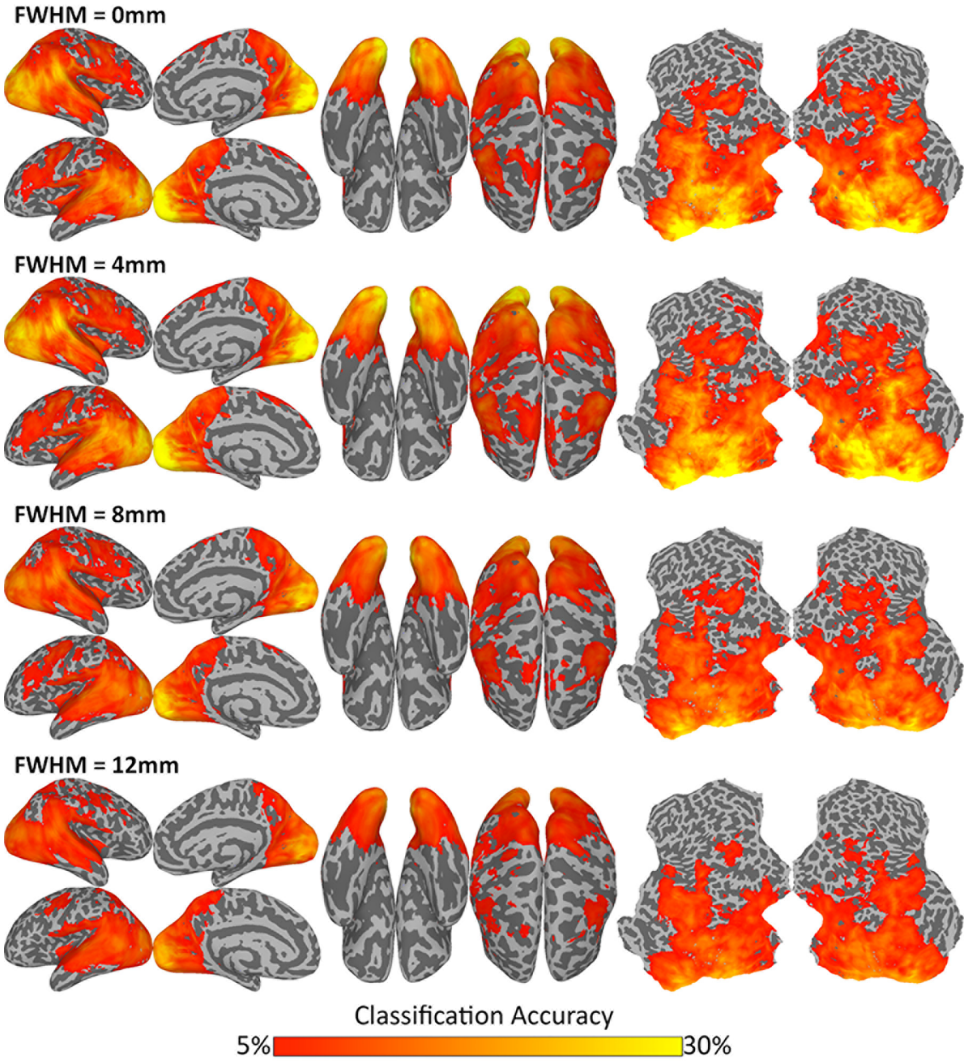


Supplementary Figure S7. Brain maps of bsMVPC of movie time segments after different levels of spatial smoothing were applied to data before hyperalignment.

*S.5. More on modeling topographies*

*S.5.1. Projecting maps of category selectivity in ventral temporal and lateral occipital cortices from the common model into individual cortical topographies*

Category-selective regions, such as the fusiform face area (FFA; Kanwisher et al. 1997; Kanwisher, 2010), the parahippocampal place area (PPA, Epstein and Kanwisher, 1998), occipital face area (OFA; Kanwisher et al. 1997; Kanwisher, 2010; Haxby et al. 1999, 2000), the lateral occipital complex (LOC; Malach et al. 1995), extrastriate body area (EBA; Downing et al. 2001), and fusiform body area (FBA; Peelen and Downing, 2005), capture elements of the coarse scale organization of object coding in the human brain. Each of these category-selective regions is defined by a contrast and is, therefore, a single dimension in the representational space.

Similarity of category-selectivity as measured by subjects' own localizer data and as estimated by other subjects' localizer data was computed by correlating (Pearson's r) those t-statistic maps for each category within a ventral visual pathway surface ROI that included VT and lateral occipital cortex.

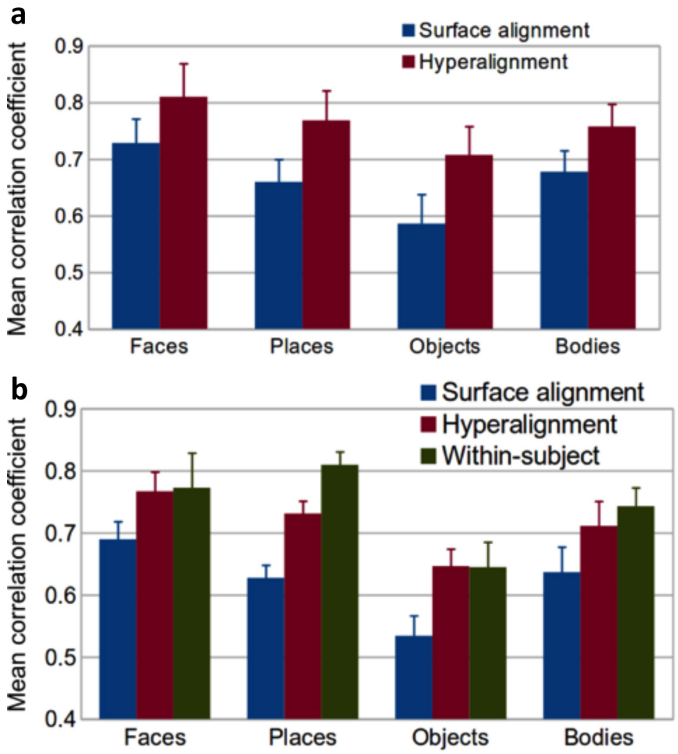


Supplementary Figure S8. Estimation of category-selectivity in the ventral visual cortex using common model. Category-selectivity was computed for faces, places, objects, and bodies using a localizer experiment. (a) Mean spatial correlations of category-selectivity maps in the ventral visual stream estimated from corresponding maps of others' after surface alignment using curvature (blue) and after whole cortex hyperalignment (red). (b) Mean spatial correlations of category-selectivity maps estimated from corresponding maps of others after surface alignment using curvature (blue), after whole cortex hyperalignment (red), and within odd and even runs of localizer experiment (green).

Reliability of the measured category-selectivity was also estimated in each subject by computing the correlation as described above between the t-statistic maps computed from odd and even runs. Correlations were also computed between the t-statistic maps estimated from other subjects' data and the t-statistic maps as measured by the odd and the even runs in each subject. These two correlations with odd and even run estimated were averaged after Fisher transformation and subjected to a bootstrapped test across all subjects for each category-selectivity contrasting correlations for anatomically aligned and hyperaligned data (Figure S8b) Maps based on subjects' own data correlated significantly higher with maps based on other subjects' data projected from common model space than with maps based on other subjects' surface curvature-aligned data (mean correlations for face-selectivity = 0.81 and 0.73, respectively, 95% CI of difference: [0.06, 0.1]; place-selectivity = 0.77 and 0.66, respectively, 95% CI of difference: [0.06, 0.15]; object-selectivity = 0.71 and 0.59, respectively, 95% CI of

difference: [0.08, 0.15]; body-selectivity = 0.76 and 0.68. respectively, 95% CI of difference: [0.06, 0.1];) (Figure S8a). Correlations of face-, place-, object-, and body-selectivity t-statistic maps between odd-even runs (faces: 0.77; places: 0.81; objects: 0.64; bodies: 0.74) were not significantly different from the same correlations between common model estimated and measured maps (95% CI of difference contained 0) except for places (95% CI of difference: [0.04, 0.11]), but were significantly different from the correlations between anatomically-aligned data estimations and the measured maps (except for faces, 95% CI of difference: [-0.02, 0.12]) (Figure S8b). These results suggest that the whole brain hyperalignment derived from the movie data captures topographies associated with the category-selectivity in the ventral visual pathway and can predict individual variations in those topographies.

*S.5.2. Projection of polar angle maps into other subjects' brains*

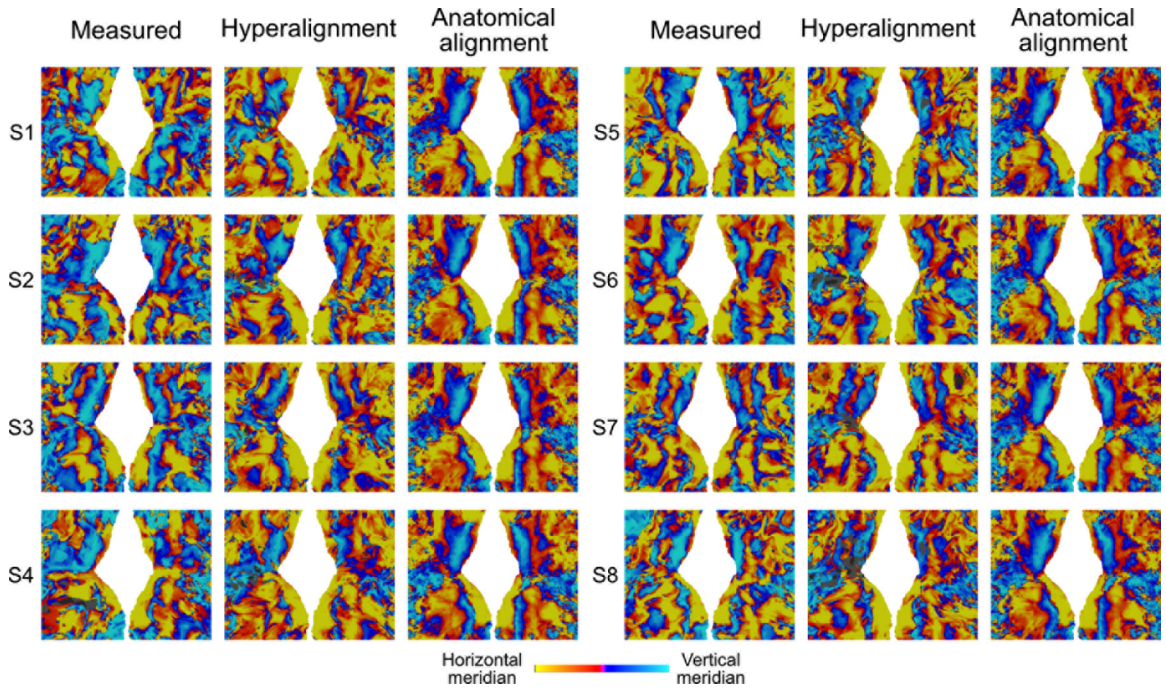


Supplementary Figure S9. Polar angle maps of individual subjects as measured from the fMRI data, as estimated from other subjects' retinotopy data in the common model space, and as estimated using anatomical alignment. Polar angle maps estimated using common model space are clearly more similar to the measured maps than are the maps estimated using anatomical alignment.

*S.6. Comparison with functional alignment*

Previously, we developed algorithms for functional alignment of cortices across subjects that used a rubber-sheet warping of the cortical manifold, similar to that used in FreeSurfer (Fischl et al. 1999) that preserves the topological contiguity of cortical nodes and was based on synchrony of responses (functional time-series alignment, FTSA; Sabuncu et al. 2010) or similarity of functional connectivity vectors (functional connectivity alignment, FCA; Conroy et al. 2009, 2013). We showed that these functional alignment algorithms improve bsMVPC of neural

responses in ventral temporal cortex to various categories of faces and objects but with accuracies that fall far short of those for wsMVPC (Conroy et al. 2013). We extend these comparisons here to a searchlight analysis of bsMVPC of movie time-segments after cortical-curvature anatomical alignment, FTSA, FCA, and hyperalignment (Supplemental Figure S10).

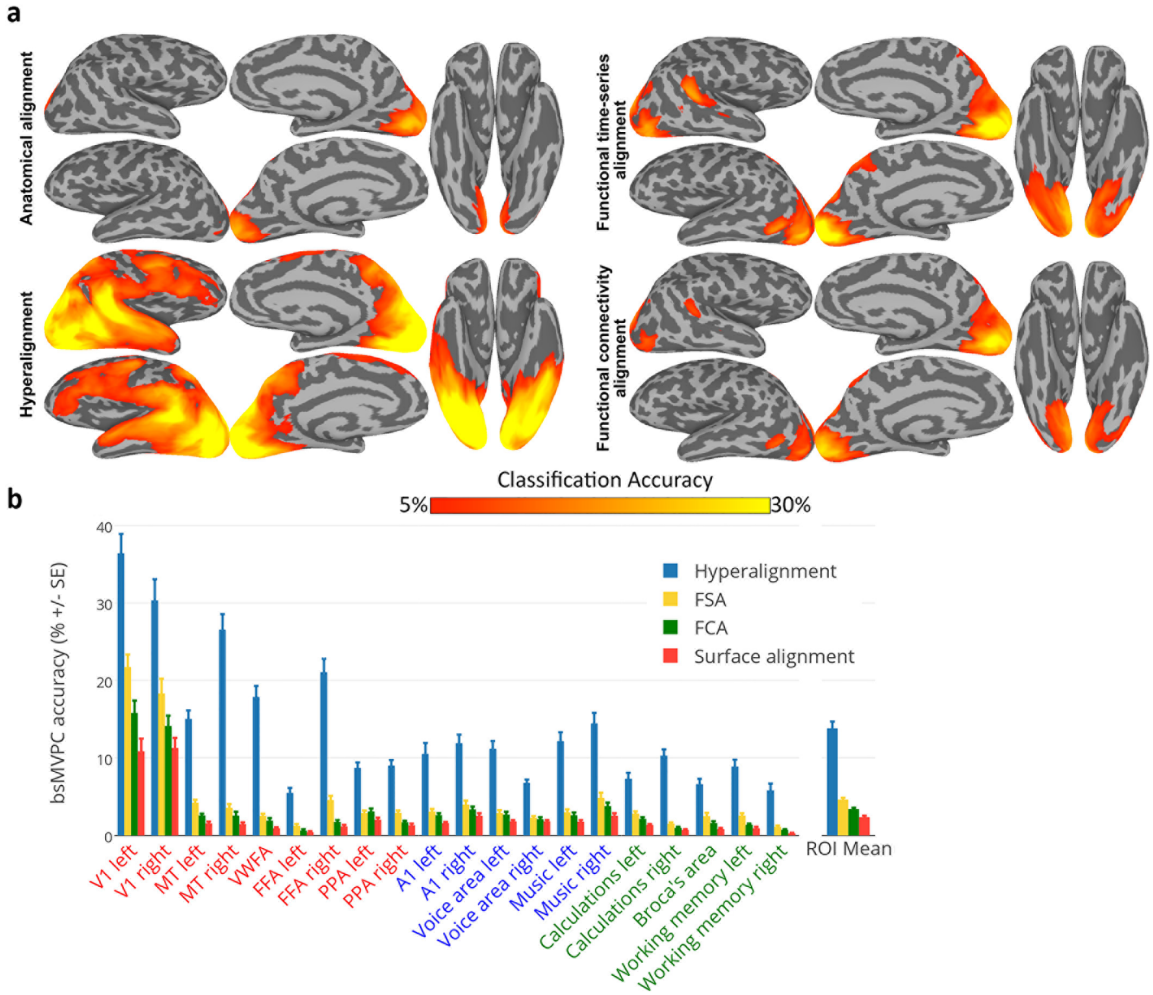


Supplementary Figure S10. Comparison of bsMVPC after FTSA and FCA – algorithms that use rubber-sheet warping of cortex that preserves topology[S15-S17] – with bsMVPC after anatomical and hyperalignment. Because FTSA and FCA use data that have been resampled into cortical nodes, the anatomical and hyperaligned data also were resampled into cortical nodes before bsMVPC for a valid comparison. Consequently, the maps for anatomical and hyperaligned data differ slightly from those in Figure 2 but are qualitatively similar. (a) Maps of bsMVPC accuracies. (b) bsMVPC accuracies for ROI searchlights (same as in other figures and detailed in Supplemental Table S1).

FTSA and FCA operate on data resampled into cortical nodes in cortical surfaces that were anatomically-aligned based on cortical curvature (Fischl et al. 1999) with a high-resolution mesh with 36,002 nodes per hemisphere. Note that we used a denser mesh for these analyses so that they were compatible with the software for FTSA and FCA, as compared to the 20,484 node mesh that we used elsewhere in this report for other cortical-surface based analyses. FTSA and FCA were performed using the methods described in Sabuncu et al. (2010) and Conroy et al. (2009, 2013). Searchlights for bsMVPC had an 18 mm radius to match the volume

of the 3 voxel radius searchlights used in the main analysis (Figure 2). Results (Supplemental Figure S10) are consistent with our previous bsMVPC analysis in VT cortex (Conroy et al. 2013), showing that bsMVPC accuracies are higher after FTSA and FCA, as compared to after anatomical alignment, but far lower than after hyperalignment.

## SUPPLEMENTAL REFERENCES

Connolly AC, Guntupalli JS, Gors J, Hanke M, Halchenko YO, Wu YC, Abdi H, Haxby JV. 2012. The representation of biological classes in the human brain. Journal of Neuroscience. 32:2608–2618.

Conroy BR, Singer BD, Haxby JV, Ramadge PR. 2009. MRI-Based inter-subject cortical alignment using functional connectivity. In Bengio Y, Schuurmans D, Lafferty J, Williams CKI, A. Culotta A, editors, Advances in Neural Information Processing Systems, volume 22, p 378-386.

Conroy BR, Singer BD, Guntupalli JS, Ramadge PR, Haxby JV. 2013. Inter-subject alignment of human cortical anatomy using functional connectivity. Neuroimage. 81:400-411.

Cortes C, Vapnik V. 1995. Support-vector networks. Machine Learning. 20:273–297.

Cox RW. 1996. AFNI: Software for analysis and visualization of functional magnetic resonance neuroimages. Computers and Biomedical Research. 29:162–173.

Downing PE, Jiang Y, Shuman M, Kanwisher N. 2001. A cortical area selective for visual processing of the human body. Science. 293:2470–2473.

Epstein R, Kanwisher N. 1998. A cortical representation of the local visual environment. Nature 392:598–601.

Fischl B, Sereno MI, Tootell RBH, Dale AM. 1999. High-resolution intersubject averaging and a coordinate system for the cortical surface. Human Brain Mapping. 8:272–284.

Haxby JV, Ungerleider LG, Clark VP, Schouten JL, Hoffman EA, Martin A. 1999. The effect of face inversion on activity in human neural systems for face and object perception. Neuron. 22:189–199.

Haxby JV, Hoffman EA, Gobbini MI. 2000. The distributed human neural system for face perception. Trends in Cognitive Science. 4:223-233.

Haxby JV, Guntupalli JS, Connolly AC, Halchenko YO, Conroy BR, Gobbini MI, Hanke M, Ramadge PJ. 2011. A common, high-dimensional model of the representational space in human ventral temporal cortex. Neuron. 72:404–416.

Kanwisher N, McDermott J, Chun MM. 1997. The fusiform face area: A module in human extrastriate cortex specialized for face perception. Journal of Neurosceicne.17, 4302–4311.

Kanwisher N. 2010. Functional specificity in the human brain: A window into the functional architecture of the mind. Proceedings of the National Academy of Sciences, USA. 107:11163-11170.

Kirby KN, Gerlanc D. 2013. BootES: An R package for bootstrap confidence intervals on effect sizes. Behavioral Research. 45:905-927.

Malach R, Reppas JB, Benson RR, Kwong KK, Jiang H, Kennedy WA, Ledden PJ, Brady TJ, Rosen BR, Tootell RBH. 1995. Object-related activity revealed by functional magnetic resonance imaging in human occipital cortex. Proceedings of the National Academy of Sciences, USA. 92:8135–8139.

Peelen, MV & Downing, PE. Selectivity for the human body in the fusiform gyrus. J. *Neurophysiol*. **93**, 603–608 (2005).

Sabuncu M, Singer BD, Conroy B, Bryan RE, Ramadge PJ, Haxby JV. 2010. Function-based intersubject alignment of human cortical anatomy. Cerebral Cortex. 20:130-140.

Yarkoni, T, Poldrack, RA, Nichols, TE, Van Essen, DC, & Wager, TD. Large-scale automated synthesis of human functional neuroimaging data. *Nature Methods*, **8**, 665–670 (2011).